Chapter 6

Enhancing the electrical and optical properties of AZO film by radiative annealing

6.1 Introduction

Solution-processed AZO films generally result in higher resistivity mainly due to inferior crystal quality and defect scattering. In general, the resistivity of AZO thin films can be further reduced by using appropriate co-dopant, increased deposition temperature, and post-deposition annealing. In most cases, spray-pyrolysis of AZO films have been carried out at substrate temperatures above 400 °C, which is often followed by an annealing step to enhance the conductivity [39,195,295–297]. The post-deposition annealing step has been carried out in an inert, vacuum, and reducing atmosphere in conventional furnaces, which take several hours to complete the thermal cycle and have a high thermal budget [66,96,298]. To mitigate this issue, recently, some non-conventional annealing has been carried out using near-infrared radiation (NIR) [299,300], microwave radiation technique (MRT) [301–303], UV laser RTA [98] and radiative annealing (RA) [304].

In radiative annealing (RA), radiation from the lamps is used as a heating source, which is a much faster and simpler way of heating thin films. The main advantage of RA is that the maximum heat is absorbed by the top layer, which reduces the time duration for annealing to a few minutes, while the substrates can remain

unaffected depending on the duration. At the same time, a controlled environment can be created inside the chamber [305–308].

Annealing in hydrogen has shown promising results in reducing the resistivity by improving the charge mobility of the AZO films. It has been demonstrated that hydrogen tends to passivate deep defects such as oxygen and zinc vacancies and Zn interstitial. In addition, hydrogen acts as a shallow donor, improving conductivity. By hydrogen incorporation, resistivities as low as ~10^{-4} Ω-cm has been achieved in the AZO films [79]. Although hydrogen incorporation has been studied in sputtered films [15, 79], reports on solution-processed films in a hydrogen atmosphere are scarce.

In this chapter, we have discussed the effect of radiative annealing at ~480°C in the presence of 5%H_2-Ar of AZO thin films deposited by spray pyrolysis. With the fast radiative annealing, the films' mobility and conductivity increased. The annealing improved mobility up to ~54 $cm^2V^{-1}s^{-1}$ in ZnO film, while the resistivity as low as has been ~2x10^{-3} Ω-cm with transparency ~94% was achieved in 2 at% Al-doped ZnO (2AZO).

6.2 Result and discussion:

6.2.1 X-ray diffraction

X-ray diffraction patterns (**Figure 6.1**) of the as-deposited and radiative annealed ZnO and AZO films could be indexed to the hexagonal wurtzite structure

(JCPDS#36-1451). All the doped samples, in as-deposited and radiatively annealed conditions, were oriented along [002] direction [202]. No trace of any additional peak corresponding to the metallic Zn, Al, or Al_2O_3 was detected.

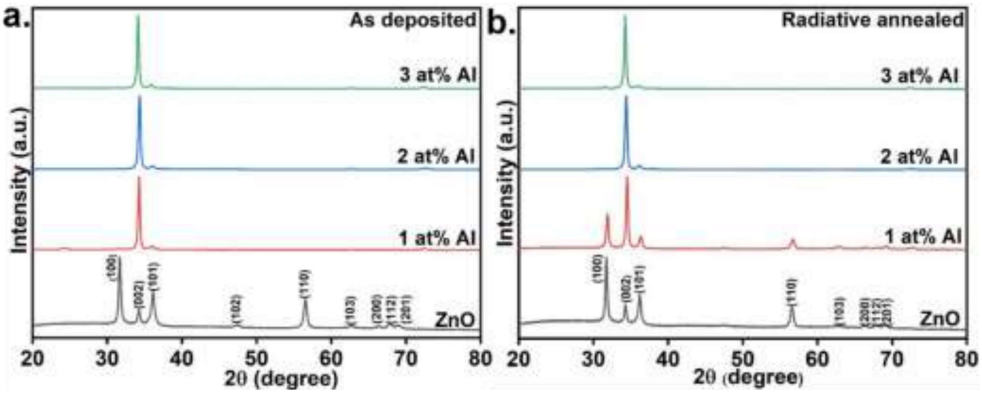

Figure 6.1 X-ray diffraction pattern a) as-deposited and b) radiative annealed pure ZnO and 1-3 at% Al-doped ZnO (AZO) films

However, in the case of pure ZnO films, in both as-deposited and radiative annealed conditions, the films had greater intensity of (100) peaks with less intense (002) and (110) peaks indicating a partial orientation along [100] direction [309]. On radiative annealing, the lattice parameter $'c'$ was reduced in all the samples (**Figure 6.2**). On the other hand, in as-deposited films, the $'c'$ parameter was reduced in the case of 2AZO, while it increased again on increasing the dopant concentration to 3AZO.

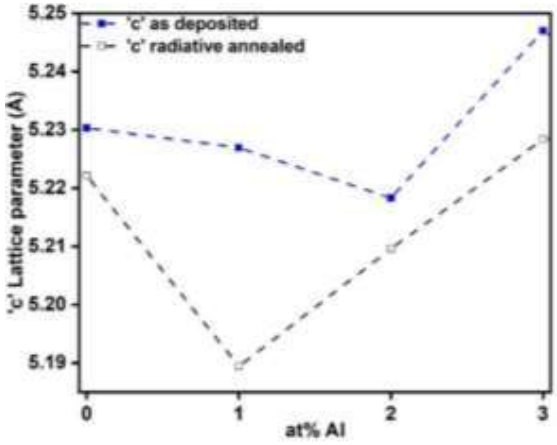

Figure 6.2 Lattice parameter of as-deposited and radiative annealed pure ZnO and 1-3AZO films

In the case of radiative annealed films, the minimum *'c'* parameter was observed for 1AZO. It was shown that the Al doping in ZnO results in a reduced *'c'* parameter because of the lower ionic radius of Al^{3+} (0.53 Å) when compared to Zn^{2+} (0.72 Å) [310]. The solubility limit of Al in ZnO is around 2%, and any excess Al tends to form the oxide and segregates to the grain boundaries [191, 311]. However, in this case, AZO films were deposited in the air; as a result, a part of Al could have oxidized, while radiative annealing in a reducing (5% H_2) atmosphere could activate some of the partially oxidized Al. In as-deposited conditions, the minimum lattice parameter was observed for 1AZO films. It is believed that the aluminum in excess of 1 at% gets oxidized, which on annealing in hydrogen atmosphere could be reduced, and a greater amount of Al could be dissolved, resulting in lattice parameter minima close to the solubility limit of 2%. Excess aluminum content in the case of 3% in both as-deposited and annealed conditions would tend to form an oxide and segregate to the grain boundary. It was reported that hydrogen

incorporation during sputtering also tends to relax the lattice by occupying the O-Zn bond-centred (H_{BC}) position and tends to passivate the oxygen vacancy (V_O-H) sites [79,312]. In this case, films were spray deposited and radiatively annealed in 5% H_2 for 10 s. There was a lesser chance for the hydrogen to go into the O-Zn bond centers; rather, it is energetically more favored for hydrogen to passivate the oxygen vacancies[54,312]. Therefore, on radiative annealing, the films became more compact, resulting in a reduced *"c"* parameter in all cases.

6.2.2 Electrical properties

The resistivity of all the samples was reduced on radiative annealing (shown in **Figure 6.3a**). In the case of as-deposited films, the resistivity reduced on doping Al, from ~211 Ω-cm for pure ZnO to ~0.165 Ω-cm on doping 2AZO. On further increasing Al concentration >2 at%, the resistivity again increased. The increase in resistivity on doping Al greater than 2% could be attributed to the segregation of excess Al in the form of Al_2O_3 at the grain boundaries [297]. On radiative annealing in a 5%H_2-Ar atmosphere, the resistivity of all the films reduced, while the minimum resistivity obtained was ~$2x10^{-3}$ Ω-cm, in the case of 2AZO film. Both the mobility and carrier concentration of all the films increased on radiative annealing, as shown in **Figure 6.3b**. After radiative annealing in the hydrogen atmosphere, deep donor V_O defect sites were substituted by hydrogen, which restored the effective mass of electrons and passivated the defects [54, 312]. The incorporation of hydrogen has also been claimed to passivate the grain boundary and form complexes with Zn_i defects resulting in reduced carrier scattering and

enhancing the films' mobility and transparency (discussed in subsection **6.2.7**) [312].

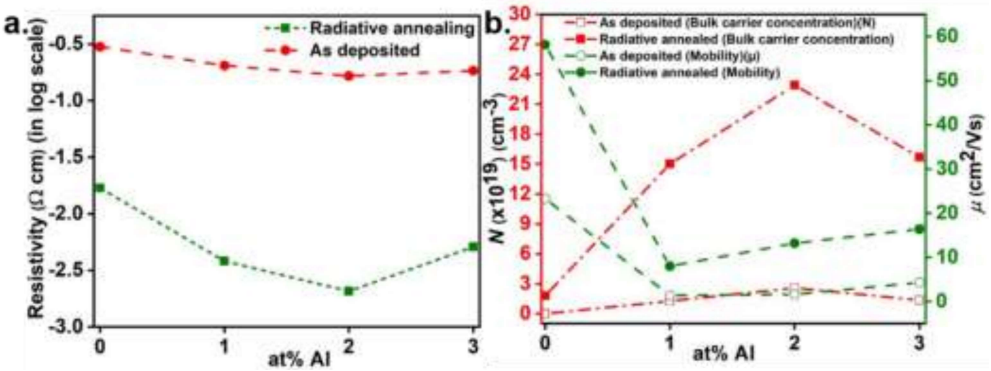

Figure 6.3 Resistivity a) bulk carrier concentration and mobility b) of as-deposited and radiative annealed pure zinc oxide and 1-3AZO thin films

At the same time, hydrogen can also act as an n-type dopant in ZnO, acting as a shallow donor and increasing the carrier concentration [54,78]. The effect of dopant concentration, in the as-deposited and annealed samples, on mobility and bulk carrier concentration is shown in **Figure 6.3b**. The mobility of ZnO increased from ~23 cm^2/Vs to the maximum mobility of ~58.14 cm^2/Vs on radiative annealing. The high mobility of the annealed ZnO films was attributed to the intrinsic nature and better defect passivation. On doping, the bulk carrier concentration increased, while the mobility was reduced due to the reduced mean free path. Although for radiatively annealed films, the mobility was reduced on doping by a factor of four (~58.14 cm^2/Vs for ZnO to ~13.2 cm^2/Vs for 2AZO films), the carrier concentration increased by more than 10 times (from ~$2x10^{19}$ for ZnO to ~$2.29x10^{20}$ cm^{-3} for 2AZO films). In the case of as-deposited films, shallow donor defects (such as Al_{Zn}) and deep-level donors (V_O) play an important role in increasing conductivity and

optical transmittance. In the case of annealed films, hydrogen substituted at V_O (H_O) and interstitial hydrogen (H_i) can play a vital role as both of them act as shallow donors [78, 312], contributing to the increase in charge carrier density. Radiative annealing of films in H_2 resulted in the passivation of V_O, Zn_i, and grain boundaries [54, 312]. Therefore, in XPS, a decrease in the concentration of oxygen in the vicinity of oxygen vacancy was observed after radiative annealing of ZnO and 2AZO (**Table 6.3**).

6.2.3 Scanning electron microscopy

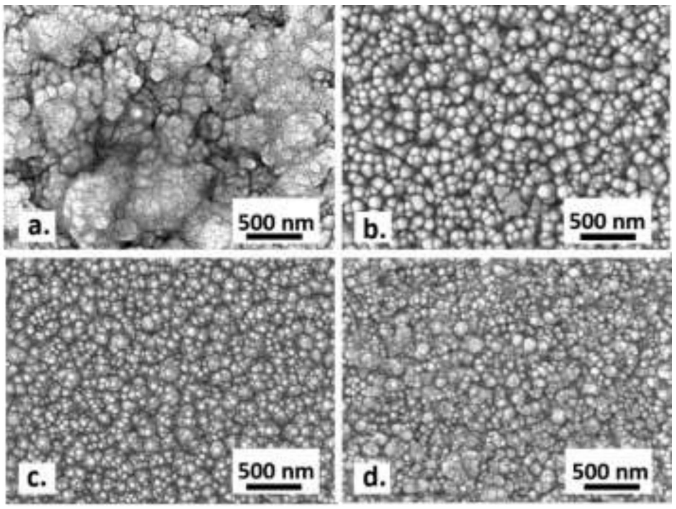

Figure 6.4 As deposited film of a) ZnO b) 1AZO c) 2AZO d) 3AZO

The morphology and coverage of the deposited and annealed films were analysed using the scanning electron microscope. Pure ZnO and 1-3 at% Al-doped films were homogeneously covering the substrate (**Figure 6.4&6.5**), while the grains were uniformly distributed over the entire film. Well-defined grain boundaries were observed without any agglomerate.

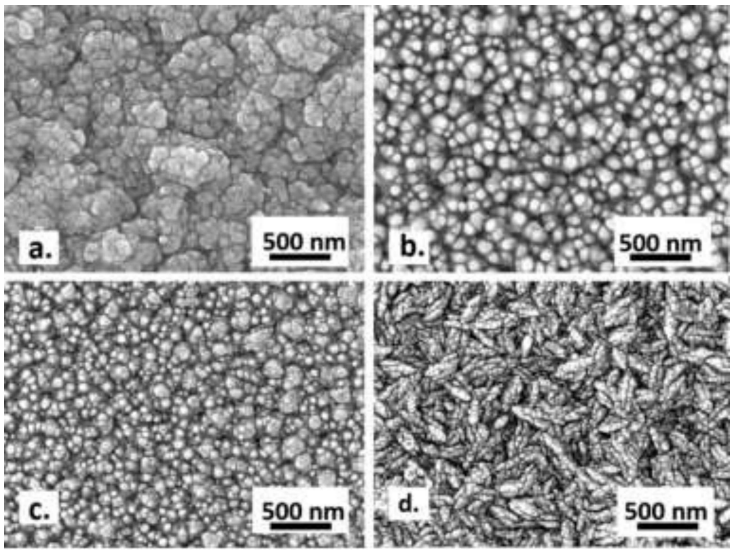

Figure 6.5 Radiative annealed film a) ZnO b) 1AZO c) 2AZO d) 3AZO

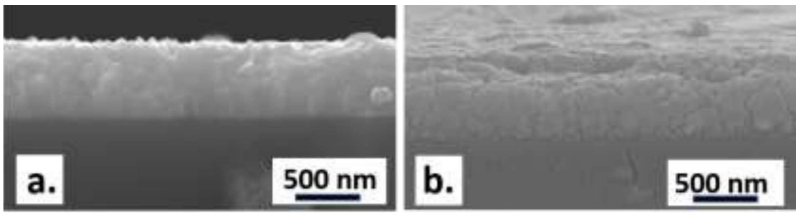

Figure 6.6 SEM images of a) cross-sectional view of as-deposited 2AZO thin film, and d) cross-sectional view of 2AZO thin film after radiative annealing

On radiative annealing (**Figure 6.5**), the microstructure became dense and compact [313]. The grain size of 2AZO film (~30-50 nm) was greater than that of pure ZnO. The thickness of all the films was between ~450 nm and ~500 nm. The cross-sectional images of as-deposited and radiative annealed 2AZO films are shown in **Figure 6.6a&b**. In the case of ZnO film, the surface was relatively rough and not

oriented, while for 2AZO the grains are aligned along the thickness, which was in line with the XRD results.

6.2.4 Raman spectroscopy

The micro-Raman spectra of the as-deposited and radiatively annealed films were recorded in the range 500-1800 cm^{-1}. The recorded Raman spectra are shown in **Figure 6.7**, while the observed peaks are listed in **Table 6.1**. ZnO has wurtzite structure having c_{6v}^4or 6mm symmetry with 2 molecules unit per unit cell; as a result, it has 12 phonon branches with 9 optical and 3 acoustic modes [314]. A_1(LO) longitudinal optical mode and second-order longitudinal optical mode 2(LO) were present in all the cases. A_1(LO) mode is a defect-induced mode associated with the presence of Zn_i and V_O, whereas $A_1$2(LO) is a characteristic wurtzite ZnO peak [204]. In the case of ZnO, A_1(LO) mode intensity could be deconvoluted into two peaks, 552 cm^{-1} and 571 cm^{-1}, related to V_O and Zn_i defects, respectively (**Figure 6.8**)[312]. The intensity of A_1(LO) lowered on radiative annealing, which was attributed to the passivation of defects due to the hydrogen incorporation during annealing. In the case of 2AZO films, the reduction in peak intensity of A_1(LO) mode was slightly lower in comparison to ZnO films, which could be attributed to the faster diffusion of hydrogen into pure ZnO [78]. The polar A_1 mode bands at 748 and 1048 cm^{-1} arising from the superimposition of longitudinal-optical and acoustic modes ((A_1((LA+TO) and A_1((LA+LO)) were also found to be considerably reduced in intensity on RA mainly due to passivation with hydrogen or elimination of defects. A similar effect was observed in the PL spectra (discussed in subsection **6.2.5**).

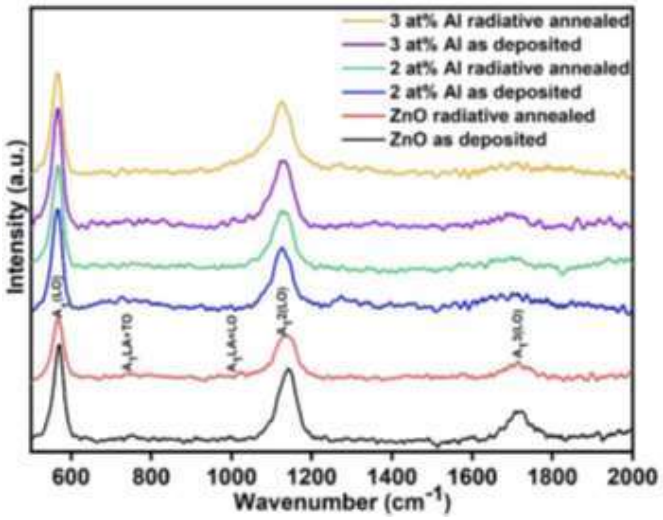

Figure 6.7 Raman spectroscopy of as-deposited and radiative annealed ZnO, 2AZO, and 3AZO films

Table 6.1 Raman spectra and peak location in case of as-deposited and radiative annealed ZnO, 2AZO, and 3AZO thin films

Sample	Mode	As deposited Centre of gravity (cm^{-1})	Radiative annealed Centre of gravity (cm^{-1})
ZnO	A_1LO	569	567
	A_1LA+TO	749	752
	A_1LA+LO	915	954
	$A_1$2(LO)	1115	1135
	$A_1$3(LO)	1716	1715
2AZO	A_1(LO)	565	564
	A_1LA+TO	728	753
	A_1LA+LO	923	895
	$A_1$2(LO)	1127	1121
	$A_1$3(LO)	1707	1696
3AZO	A_1(LO)	565	565
	A_1LA+TO	742	758
	A_1LA+LO	915	922
	$A_1$2(LO)	1126	1123
	$A_1$3(LO)	1701	1710

Full range spectra of as-deposited and radiatively annealed 2AZO film (**Figure 6.9**) show that E_2 (high) mode, which is generally related to the lattice strain, in the as-deposited film is at 445 cm^{-1}, shifted to a higher wave number 480 cm^{-1} indicating to the presence of some compressive stress in the film. It agreed with the XRD results where (002) peak shifts to a higher angle on radiative annealing.

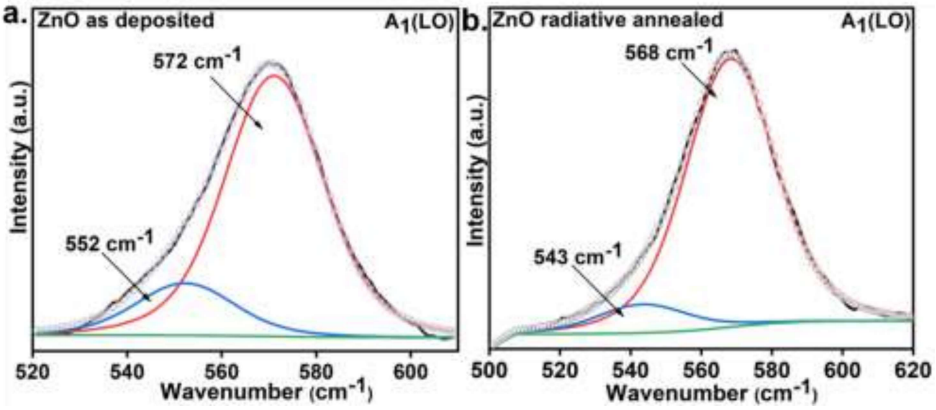

Figure 6.8 As deposited and radiative annealed deconvoluted A_1(LO) peak of ZnO

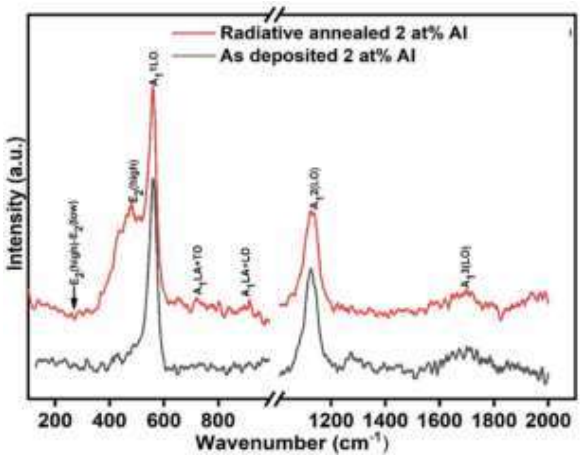

Figure 6.9 Raman spectrum of 2AZO as-deposited and radiative annealed

6.2.5 Photoluminescence

Photoluminescence spectra obtained for ZnO and AZO films are presented in **Figure 6.10a**. Apart from the typical near band-edge (NBE) emission (360-380 nm), a broad visible emission (387-530 nm) originating from defects levels encompassing violet, blue, cyan, and green emissions (deconvoluted and listed in **Figure 6.10b**).

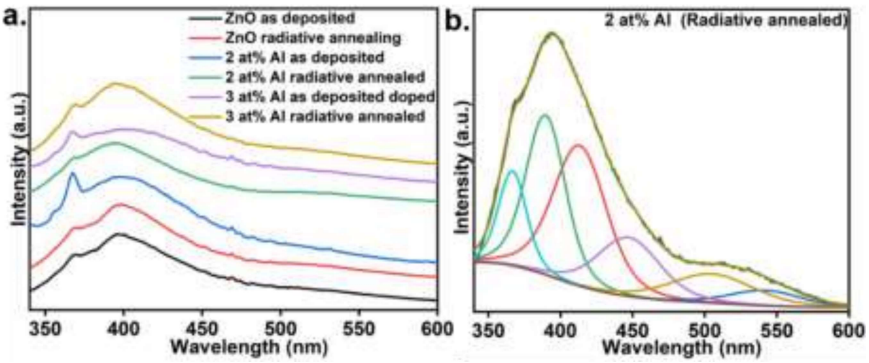

Figure 6.10 a) PL spectra of as-deposited and radiative annealed pure ZnO and 2-3AZO, and b) deconvoluted peaks of radiative annealed 2AZO

The defect intensity ratio of ZnO, 2AZO, and 3AZO is shown in **Table 6.2**. In general, the intensity of peaks in the visible range reduced on radiative annealing, while near band edge (NBE) emission became intense. The integrated intensity of the defect peaks normalized against the NBE emission is listed in **Table 6.2**. I_{Violet}/I_{NBE}, $I_{Blue}/I_{NBE,}$ and I_{Green}/I_{NBE} ratios decreased on radiative annealing.

Table 6.2 Defect energy location in as-deposited and radiative annealed ZnO, 2AZO, 3AZO thin films

	As deposited			Radiative annealed		
Sample	**Peak location (eV)**	**Defect**	**I_{defect}/I_{NBE}**	**Peak location (eV)**	**Defect**	**I_{defect}/I_{NBE}**
ZnO	3.17 (Violet)	Zn_i	6.16	3.19 (Violet)	Zn_i	2.44
	2.95 (Blue)	Zn_i (+2/+1)	3.01	2.97 (Blue)	Zn_i (+2/+1)	2.45
	2.74 (Cyan)	Zn_i (+1/+0)	1.96	2.75 (Cyan)	Zn_i (+1/+0)	2.21
	2.44 (Green)	V_o	2.65	2.38 (Green)	V_o	1.28
2AZO	3.20 (Violet)	Zn_i	4.02	3.18 (Violet)	Zn_i	1.67
	3.00 (Blue)	Zn_i (+2/+1)	3.90	3.03 (Blue)	Zn_i (+2/+1)	1.96
	2.81 (Cyan)	Zn_i (+1/+0)	4.01	2.85 (Cyan)	Zn_i (+1/+0)	2.47
	2.50 (Green)	V_o	3.93	2.40 (Green)	V_o	1.09
3AZO	3.16 (Violet)	Zn_i	2.62	3.13 (Violet)	Zn_i	1.27
	2.95 (Blue)	Zn_i (+2/+1)	2.96	2.97 (Blue)	Zn_i (+2/+1)	1.28
	2.73 (Cyan)	Zn_i (+1/+0)	2.33	2.83 (Cyan)	Zn_i (+1/+0)	1.2
	2.40 (Green)	V_o	1.77	2.47 (Green)	V_o	1.22

The violet emission peaks at ~387-400 nm (3.20-3.13 eV) were attributed to the Zn_i close to the crystallite boundaries ZnO-H and AZO-H film [66]. The narrow blue emission peaks, observed in the range of ~415-420 nm (2.95-2.97 eV), were due to Zn_i^{+2} to Zn_i^{+1} transition, the cyan emission peaks at ~435-450 nm (2.73-2.85 eV) were related to Zn_i^{+1} to Zn_i^{*} transition, while the green emission peaks at ~500-525 nm (2.38-2.47 eV), could be attributed to the presence of V_O^{++} [312]. All the defect

peak intensities were normalized against the NBE peak intensity (**Table 6.2**). All the defect-related PL peaks became less intense on radiative annealing in H_2. For instance, I_{Violet}/I_{NBE} ratios exhibit a ~2.4-fold decrease while the I_{Blue}/I_{NBE} intensity ratio decreased by two folds after radiative annealing suggesting the formation of Zn_i-H (Zn_i^+ exist at the surface) in case of both ZnO and AZO films. This shows that the passivation of Zn_i defects on radiative annealing in H_2 [272,273]. I_{Green}/I_{NBE} intensity ratio decreased by more than 3-fold on radiative of 2AZO film, which indicated the effective passivation of oxygen vacancies. Radiative annealing effectively passivated both the Zn_i-related defects and oxygen vacancies (V_O) in AZO films[315,316].

6.2.6 X-ray photoelectron spectroscopy

For all the films the O1s peak XPS peak was asymmetric with a tail towards the higher binding energy. The high-resolution O1s peak could be deconvoluted into three peaks: O_I (at 530.1±0.2 eV), O_{II} (~530.8 eV), and O_{III} (~531.8 eV) as shown in The peak O_{III}, on the other hand, was attributed to the oxygen (O_{Ads}) chemically adsorbed species such as water, $-OH^-$ or $-CO_3^{-2}$. It has been established that the V_O plays an important role in deciding the electrical properties of the ZnO-based thin films [237]. For comparison, the concentration of adsorbed oxygen and oxygen associated with the vacancy was normalized against the lattice oxygen peak. The intensity ratio O_{Ads}/O_{Lat} increased on radiative annealing of ZnO, while the ratio reduced in the case of AZO films [315,317] (listed in **Table 6.3**). This happened due to the greater electron affinity of aluminum for oxygen. O_{Vac}/O_{Lat} ratio, on the other hand, reduced slightly on radiative annealing due to the passivating effect of

hydrogen. This was consistent with the Raman and PL spectroscopy results (see subsections **6.2.4** and **6.2.5**).

Figure 6.11. The peak O_I was attributed to the lattice oxygen, while the higher binding energy component O_{II} was associated with oxygen ions in the oxygen-deficient region (O_{Vac}).

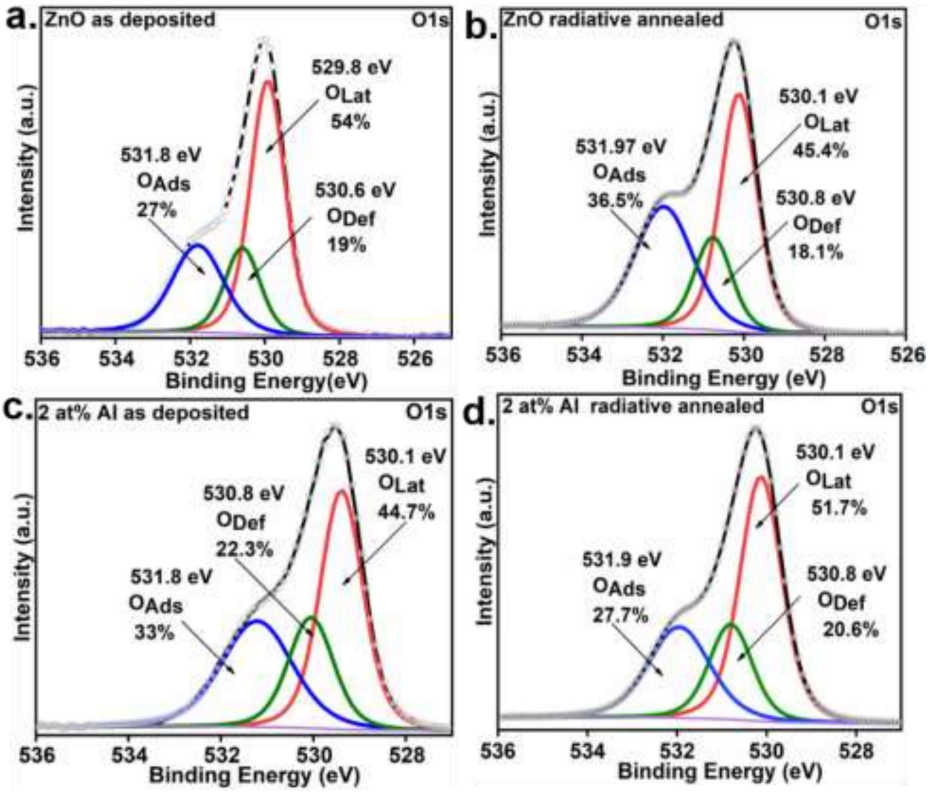

Figure 6.11 XPS of O1s orbital of a) ZnO as deposited b) ZnO radiatively annealed c) 2AZO as deposited d) 2AZO radiative annealed

At the same time, the hydrogen incorporation (H_O) acted as a shallow donor resulting in enhanced carrier density [317], as shown in subsection **6.2.2**.Zn2p XPS peaks of the as pure ZnO films were centered at 1021.26±0.05 eV and 1044.30±0.05

eV, corresponding to $Zn2p_{3/2}$ and $Zn2p_{1/2}$ [33], which on annealing shifted to the higher binding energies 1021.86 eV and 1044.97 eV, respectively as shown in **Figure 6.12a**.

Table 6.3 O_{Ads}/O_{Lat} and O_{Def}/O_{Lat} obtained from deconvoluted O1s XPS peak of pure ZnO and 2AZO films as deposited and radiative annealed

Sample	O_{Ads}/O_{Lat}	O_{Def}/O_{Lat}
ZnO (as deposited)	0.50	0.35
ZnO (Radiative Annealed)	0.79	0.40
2AZO (as deposited)	0.74	0.50
2AZO (Radiative Annealed)	0.54	0.40

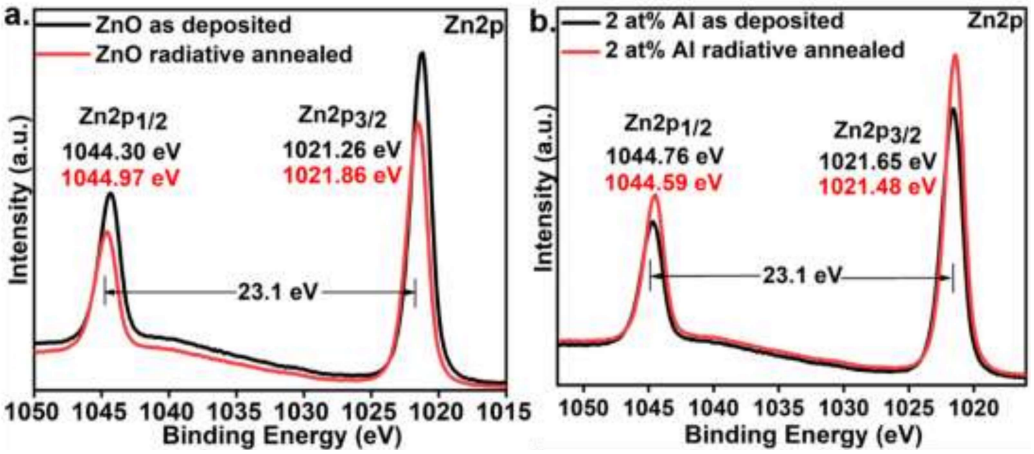

Figure 6.12 XPS of Zn2p orbital pure ZnO a) and 2AZO thin film b) as-deposited and radiative annealed

On the other hand, an opposite shift of ~0.17 eV in Zn2p peaks towards lower binding energy was observed on radiative annealing of 2AZO, as shown in **Figure 6.12b**.For 2AZO, Zn2p3/2 and Zn2p1/2 peaks are centred at 1021.65eV and

1044.76 eV, which was shifted to 1021.48 and 1044.59 eV on radiative annealing [315,318]. The opposite shift in the binding energy of the Zn 2p in pure ZnO and AZO was observed earlier and was attributed to the presence of Al at the surface site [106,234,280]. Formation of O-Zn bond with the adsorbed oxygen due to radiative annealing; as a result, the Zn2p peaks shifted towards higher binding energy. On the other hand, the terminating surface contains more electronegative Al atoms and Zn, which form stronger bonds with oxygen. The affinity of Al towards O results in increased formation of Zn-Zn bonds (lowering Zn2p binding energy) and reduced the O_{Ads}/O_{Lat} fraction, as listed in **Table 6.3**. The Al2p peaks centered at 74.0 ± 0.1 eV [106], as shown in **Figure 6.13a**, indicated the Al substitution of Zn in the ZnO lattice. On radiative annealing of AZO films, Al2p peaks shifted towards lower binding energy (73.67±0.1 eV) [106], as shown in **Figure 6.13b**. Shifting of the Al 2p peak to lower binding energy was attributed to a partial reduction of alumina, resulting in dopant activation in the presence of hydrogen at a higher temperature of ~480 °C [319]. It has been established that defects such as Zn_i, Al_{Zn},$V_{O,}$ and H_O play a major role in determining the electrical properties of ZnO TCOs. The presence of these doner defects leads to the Fermi level shifting towards the conduction band. On radiative annealing, the Fermi edge of the ZnO films shifted from 2.25 eV to 2.66 eV on radiative annealing (**Figure 6.14a**), while the Fermi edge of 2AZO films shifted from 2.52 eV to 3.06 eV on radiative annealing (**Figure 6.14b**).

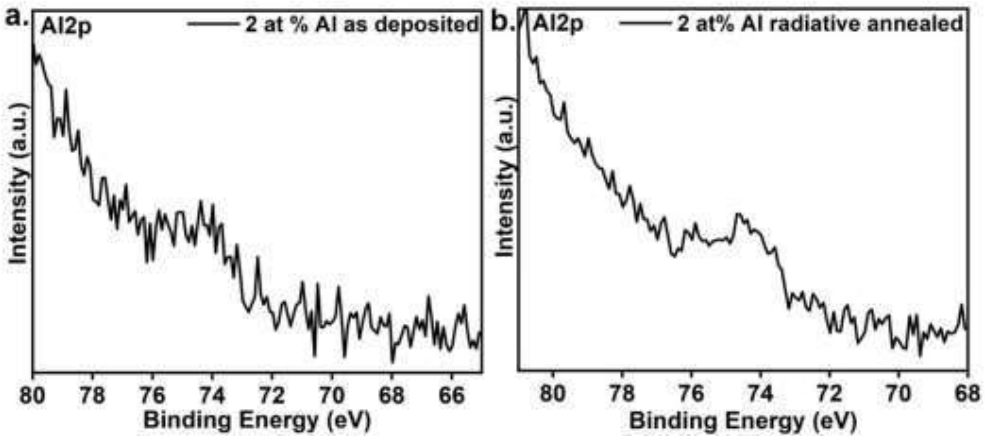

Figure 6.13 X-ray photoelectron spectroscopy of Al2p orbital a) 2AZO as deposited b) 2AZO after radiative annealing

Fermi edge moving towards CBM indicates increased carrier concentration which was also reflected in the hall measurement presented in subsection **6.2.2** [39].

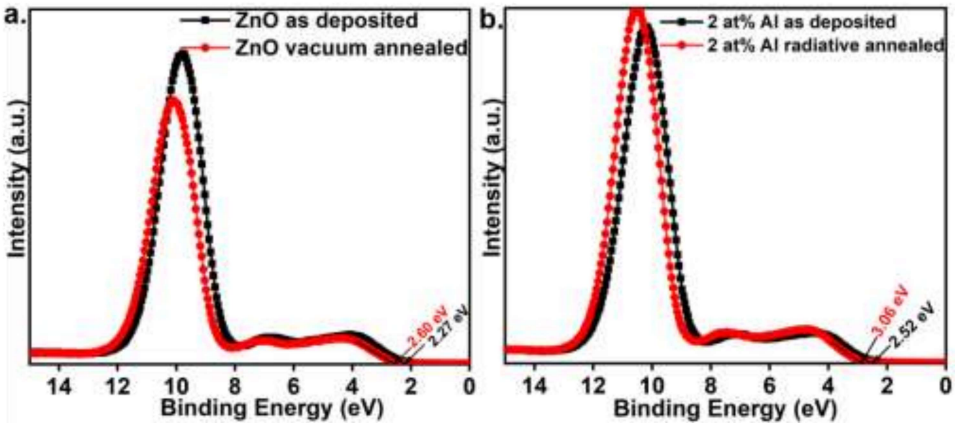

Figure 6.14 Valence band XPS of Zn3d orbital of a) pure ZnO, and b) 2AZO films as deposited and radiative annealed

6.2.7 Optical properties

UV–visible spectroscopy was carried out to characterize the optical properties of the films. **Figure 6.15a** shows the transmittance spectra of the as-deposited ZnO and AZO films. The transparency (at 550 nm) of the as-deposited ZnO film was 75%, which increased with doping to ~90% for 2AZO films, while a lower transmittance (~82% at 550 nm) was observed for 3AZO films. A similar trend was reported earlier [79].

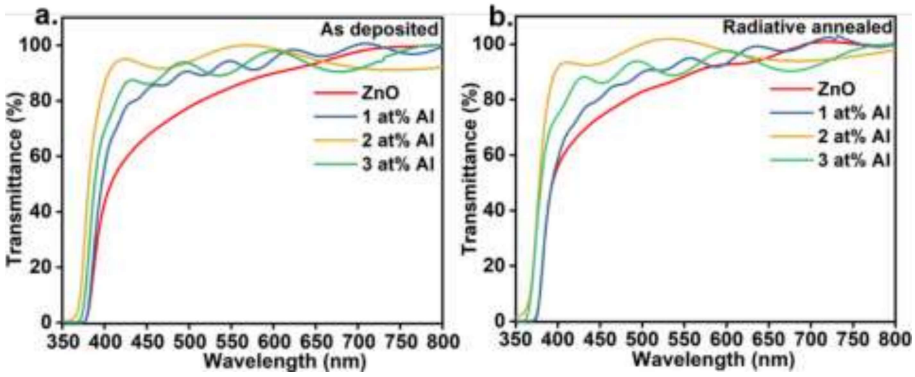

Figure 6.15 a) As deposited, and b) radiative annealed transmittance of the pure ZnO and 1-3AZO films

Radiative annealing significantly improved the transmittance of pure ZnO films (from ~75 to 80% at 550 nm), while only marginally improving in transmittance of doped films (**Figure 6.15b**). The increased transparency of the annealed film could be attributed to the passivation of grain boundaries and defects. The optical bandgap energy (E_g) was estimated using the Tauc plot, as shown in the inset of **Figure 6.16a**. In as-deposited films, optical bandgap increased with Al-doping up to 2 at%. The optical bandgap of 2AZO films increased to 3.28 eV, while on increasing Al doping to 3 at%, the bandgap again narrowed to 3.25 eV, which was attributed to

the oxidation of excess Al [320,321]. On radiative annealing, the bandgap increased to 3.22 eV for ZnO and 3.34 eV for 2AZO films (shown in (**Figure 6.16b**). It was observed that the hydrogen atmosphere could partially reduce the alumina. Both radiative annealing and doping increased n-type carrier concentration, which partially occupied the energy levels close to the conduction band minimum and increased the optical bandgap [97,184,270,271].

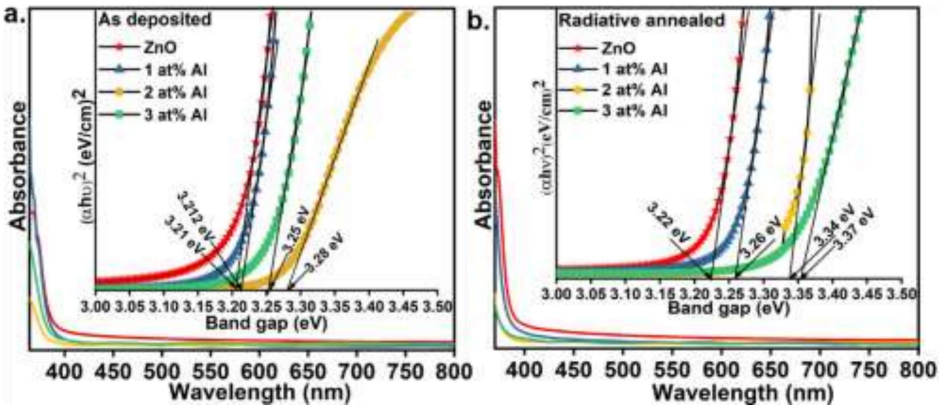

Figure 6.16 a) As deposited, and b) radiative annealed absorbance and Tauc plot (inset) of the pure ZnO and 1-3AZO films

Therefore, a significant increase in optical bandgap was observed in 2AZO (from 3.28 eV in the as-deposited condition to 3.34 eV on annealing). However, since 2% is the solubility limit for Al dissolution in ZnO, only a marginally greater bandgap was observed for radiative annealed 3AZO films. The figure of merit (FOM) of the as-deposited and radiative annealed film is shown in **Figure 6.17**. It can be observed that 2AZO film had the highest FOM of 0.011, which compares well with the vapor-based processed films [15,79].

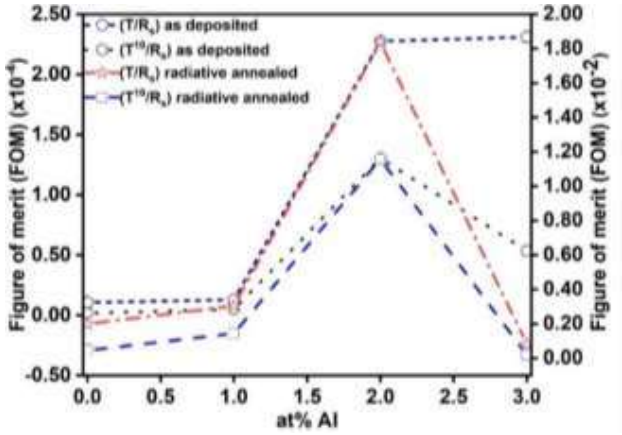

Figure 6.17 Figure of merit of as-deposited and radiative annealed pure ZnO and 1-3AZO thin films

6.2.8 Concluding Remarks

Radiative annealing in the presence of 5%H_2+Ar was used to improve transparency, and lower resistivity of the solution spray deposited ZnO-based TCOs. A quick 10 s radiative annealing can improve the optical and electrical properties. Transparency was as high as ~94% with resistivity as low as ~2x10^{-3} Ω-cm achieved for 2AZO films. Radiative annealing for 10 s improved the crystallinity and passivated the defects resulting in improved mobility (up 58.14 cm^2/Vs in pure ZnO films). At the same time, annealing in H_2 also activated a greater amount of dopant and acted as a source for additional carriers resulting in a carrier concentration as high as ~2.29x10^{20} cm^{-3} for 2AZO films. Therefore, radiative annealing can be further explored as a potential post-deposition annealing technique for conductivity and transparency close to that obtained from vapor-based deposition technologies.